

Comparisons of TDM and FDM Pilot Signals for Phase Noise Estimation with High-Order QAM for DFT-Spread OFDM

Ryota Kuribayashi
Tokyo City University
Tokyo, Japan

Mamoru Sawahashi
Tokyo City University
Tokyo, Japan

Abstract—This paper presents comparisons of time division multiplexing (TDM) and frequency division multiplexing (FDM) based pilot signal multiplexing methods for estimating the time-varying phase noise (PN) in a high-order QAM scheme for discrete Fourier transform (DFT)-spread orthogonal frequency division multiplexing (DFT-S-OFDM). Computer simulation results show that the peak-to-average power ratio at the complementary cumulative distribution function of 10^{-4} of DFT-S-OFDM with FDM pilot multiplexing is increased by approximately 1.8 dB and 1.2 dB compared to that for DFT-S-OFDM with a TDM based pilot signal and that for DFT-S-OFDM without a pilot signal, respectively, for 256QAM. We also show that the required received signal-to-noise ratio (SNR) satisfying the bit error rate (BER) of 10^{-8} for the TDM based pilot signal is decreased by approximately 1.1 dB, 1.2 dB, and 1.3 dB compared to that with the FDM based pilot signal for the low-density parity-check (LDPC) coding rate of 1/2, 3/4, and 8/9, respectively, for 256QAM assuming the same frequency bandwidth. Hence, we show that the TDM based pilot signal for PN estimation achieves superior performance to that for the FDM based pilot signal although FDM based pilot multiplexing has the potential for improvement by using elaborate cancellation of single-carrier distortion.

Index Terms—DFT-spread OFDM, pilot signal multiplexing, phase noise, extended Kalman filter, mobile backhaul links

I. INTRODUCTION

The discrete Fourier transform (DFT)-spread orthogonal frequency division multiplexing (OFDM) (DFT-S-OFDM) waveform is adopted in the 3GPP Long Term Evolution (LTE) uplink and in the New Radio (NR) uplink with a single-stream transmission [1]. DFT-S-OFDM assigns a single-carrier (SC) signal to the allocated transmission bandwidth in the frequency domain (FD) and has radio parameters in common with the OFDM waveform. DFT-S-OFDM also has affinity to FD equalization at a receiver. Furthermore, OFDM based NR radio interfaces are used for backhaul links between a donor base station (BS) and a relay BS in addition to the access links in the 3GPP integrated access and backhaul (IAB) specifications [3].

Taking into consideration the increasing traffic demands including IoT traffic in cellular systems, further improvement in spectral efficiency in the sub-6-GHz bandwidths is imperative. In addition, taking full advantage of the millimeter-wave bands is necessary. Taking into account the significantly large path loss in the millimeter-wave bands, DFT-S-OFDM is a promising waveform for mobile backhaul links as well as

access links in the beyond-5G systems due to its low peak-to-average power ratio (PAPR) feature [4], [5]. One of the most challenging issues is a time-varying phase noise (PN) that arises in a local oscillator of a BS and set of user equipment (UE). A pilot signal that is referred to as a reference signal (RS) in the NR specifications is required to estimate time-varying PN precisely. In time division multiplexing (TDM), a pilot signal that is multiplexed in a dedicated DFT-spread block or DFT-S-OFDM symbol increases the overhead and lacks tracking accuracy for the time-varying PN. In the NR specifications, therefore, a TDM based phase tracking reference signal (PTRS) that is multiplexed with data symbols within a DFT-spread block before DFT precoding is specified for estimating the PN and carrier frequency offset [1]. The TDM based PTRS has merits including a low PAPR compared to a frequency domain multiplexing (FDM) one. Meanwhile, the tracking accuracy for the time-varying PN of TDM based pilot signal multiplexing is considered to be potentially inferior to that for FDM based pilot signal multiplexing in which pilot symbols are multiplexed continuously in the time domain (TD) at certain subcarrier locations. Using the FDM based pilot signal for the purpose of channel estimation was proposed for DFT-S-OFDM [6]. It was proven in [6] that the FDM based pilot achieves accurate tracking performance for the time-varying channel response at the sacrifice of an increase in the PAPR. Focusing on phase-noise compensation (PNC) for high-order QAM, [7] proposed an effective PNC scheme comprising pilot symbol assisted (PSA) PNC based on the Wiener filter and residual PNC using a phase locked loop. In [7], a TDM based pilot signal was used for SC transmission, and a very low bit error rate (BER) was shown with a low computational complexity level for 256QAM. In [9], we proposed a two-step PNC scheme that comprises PSA PNC in the TD using FDM pilot signals [8] and iterative extended Kalman filter (EKF) PNC (PSA-EKF PNC hereafter) for OFDM backhaul links. Based on the structure in [9], we proposed PNC that comprises PSA PNC and iterative PNC using the EKF including cancellation of the SC distortion due to puncturing in multiplexing the FDM pilot signals for DFT-S-OFDM [10]. The pilot structure for PN estimation is very important in the radio interface as well as for other purposes including channel estimation and channel state information

estimation. However to the best knowledge of the authors, a better multiplexing method between TDM and FDM of the pilot signal for estimating the PN has not yet been reported for high-order QAM schemes for DFT-S-OFDM.

This paper presents comparisons of TDM and FDM based pilot signal multiplexing methods for estimating the time-varying PN for high-order QAM for DFT-S-OFDM. The features of the investigation in this paper are as follows. The first point is that we target high quality reception such as the BER of 10^{-8} with high-order QAM for DFT-S-OFDM aiming at application to mobile backhaul links and access links yielding, *e.g.*, ultra reliable low latency communication (URLLC) services. The second point is that two-step PSA-EKF PNC is used that comprises PSA PNC in the TD and iterative PNC using the EKF employing demapping bits before the low-density parity-check (LDPC) decoder. This is because it achieves the low BER of 10^{-8} with a relatively low level of computational complexity. The third is that we provide a fair comparison assuming the same frequency bandwidth including the frequency resources required for additional signals and pilot signals. The rest of the paper is organized as follows. In Section II, we describe a transmitter structure with TDM and FDM pilot multiplexing for PN estimation for DFT-S-OFDM. Next, Section III describes the PSA-EKF PNC receiver structure. Section IV presents the computer simulation results. Finally, Section V gives our conclusions.

II. TRANSMITTER STRUCTURE USING TDM AND FDM BASED PILOT SIGNALS FOR PN ESTIMATION FOR DFT-S-OFDM

Fig. 1 shows a transmitter structure with FDM and TDM based pilot signals for PN estimation for DFT-S-OFDM. We use the LDPC code with the coding rate of $R = 1/2, 3/4,$ and $8/9$ for digital video broadcasting in ETSI [11]. We use $R = 8/9$ basically. In the case of $R = 8/9$, 14,232 bits are encoded using the Bose-Chaudhuri-Hocquenghem (BCH) code with 12-bit correction to be 14,400 bits [11]. The respective BCH-coded bits are LDPC-encoded and bit-interleaved to generate a code block with 16,200 bits. The LDPC-coded bits after interleaving are grouped into Γ groups with each group containing ρ bits as $\{[b_{0,0}, \dots, b_{0,\rho-1}], \dots, [b_{\Gamma-1,0}, \dots, b_{\Gamma-1,\rho-1}]\}$ (Γ is the number of groups corresponding to the number of symbols and ρ is the number of coded bits in each group). The $\rho = 8$ bits of each group are mapped to a complex symbol among the Gray-encoded 256QAM constellations. We assume a slot structure based on the NR specifications, in which one slot comprises 14 DFT-S-OFDM symbols. In this paper, we multiplex the data symbols in 13 DFT-S-OFDM symbols except for the first one. Here, 2,025 LDPC-coded 256QAM symbols are divided into 13 blocks.

(1) FDM based pilot multiplexing

We use the FDM based pilot multiplexing method for DFT-S-OFDM reported in [12] and [13]. We denote the data symbol sequence of each block as $\mathbf{s}_D = [s_D(0), s_D(1), \dots, s_D[N_D - 1]]$. Here, $s_D(\bar{n})$ is the 256QAM symbol where \bar{n} denotes a symbol index ($0 \leq \bar{n} \leq N_D - 1$). The N_D value is 161 after padding dummy symbols to the data symbols.

As shown in Fig. 1(a), we add signal “0” in the $M \times L$ symbol duration in front of data symbol block \mathbf{s}_D [12], [13]. Here, M denotes the number of subcarriers in which the FDM pilot is multiplexed and L denotes the number of blocks each with signal “0” in the M symbol duration. The symbol sequence after adding signal “0”, \mathbf{u}_t , is represented as $\mathbf{u}_t = [\mathbf{0}_{1:M \times L} \ \mathbf{s}_D] = [u(0), \dots, u(N_{DFT} - 1)]$. Here, $\mathbf{0}_{1:M \times L}$ denotes a vector comprising the $M \times L$ symbols of “0”. In normal DFT-S-OFDM without FDM based pilot multiplexing, the DFT size, N_{DFT} , becomes $N_{DFT} = N_D$. Meanwhile, N_{DFT} becomes $N_{DFT} = M \times L + N_D$ at the cost of an increase in the transmission bandwidth. We let the DFT computation with $N_{DFT} \times N_{DFT}$ be $\mathbf{F}_{N_{DFT}}$, *i.e.*, $U(\bar{k}) = \frac{1}{\sqrt{N_{DFT}}} \sum_{\bar{n}=0}^{N_{DFT}-1} u(\bar{n}) \exp\left(-\frac{j2\pi\bar{k}\bar{n}}{N_{DFT}}\right)$. TD symbol sequence \mathbf{u}_t is converted to FD signal \mathbf{U}_f as $\mathbf{U}_f = \mathbf{F}_{N_{DFT}} \mathbf{u}_t$. The number of subcarriers in the FD signal is $M \times L + N_D$ (note that we use the term subcarrier for the frequency component of DFT-S-OFDM in this paper). We puncture the M subcarrier signals every $L + Q$ subcarrier interval and multiplex FDM pilot symbols $p(m)$ ($m = 0, \dots, M - 1$) as $U_f(m(L + Q)) = p(m)$ ($m = 0, 1, \dots, M - 1$). The SC signal after puncturing and multiplexing of the FDM based pilot symbols, $S_f(\bar{k})$, is represented in the next equation.

$$S_f(\bar{k}) = \begin{cases} p(\bar{k}/(L + Q)) & \text{if } \bar{k} = m(L + Q), \quad m = 0, \dots, M - 1 \\ u_f(\bar{k}), & \text{otherwise} \end{cases} \quad (1)$$

In this paper, we set $M = 23$ based on the results in [9]. We employ a Zadoff-Chu sequence for the FDM based pilot sequence [14]. After inserting a zero signal in both sides of $M \times L + N_D$ subcarriers including the FDM pilot subcarriers to generate 256-subcarrier signals S_k ($0 \leq k \leq 255$), the FD signals are fed into an inverse fast Fourier transform (IFFT) to generate the DFT-S-OFDM signal as $\mathbf{s}_t = \mathbf{F}_{N_{FFT}}^H \mathbf{S}_f$. Here, $\mathbf{F}_{N_{FFT}}^H$ denotes an IFFT matrix and each component is given as $s_n = \frac{1}{\sqrt{N_{FFT}}} \sum_{k=0}^{N_{FFT}-1} S_k \exp\left(\frac{j2\pi kn}{N_{FFT}}\right)$ where $N_{FFT} = 256$ is the IFFT size. Finally, a cyclic prefix is appended at the beginning of each DFT-S-OFDM symbol.

(2) TDM based pilot multiplexing

In the NR specifications, six sets of the number of PTRS groups within a single DFT-S-OFDM symbol and the number of samples per PTRS group are specified according to the allocated number of resource blocks [1], [2]. As shown in Fig. 1(b), we multiplex pilot symbols before the DFT in the TD according to the multiplexing method of the PTRS in the NR specifications. However, to make fair the investigation with FDM pilot multiplexing assuming the same available transmission bandwidth, we consider a number of pilot symbol blocks within a single DFT-S-OFDM symbol that is significantly larger than that in the NR specifications. In this paper, we assume that the number of pilot symbols per pilot symbol block is four or five, which is equivalent to the PTRS in the NR specifications. As a result, the number of pilot symbol blocks within DFT-S-OFDM becomes 5, 12, 17, and 23 for $L = 1, 2, 3,$ and 4 , respectively. The corresponding number of data

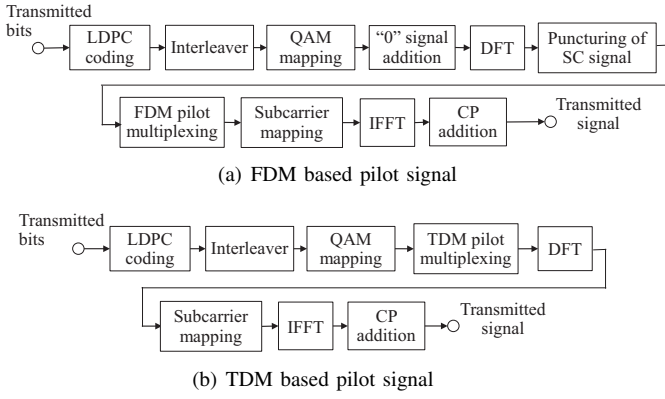


Fig. 1. Transmitter structure with TDM and FDM based pilot signals for PN estimation for DFT-S-OFDM.

symbols between the contiguous pilot symbol blocks is 32 or 33, 14, 10, and 7. Hence, according to the increase in the L value, the tracking performance of the TDM pilot multiplexing for the PN is improved. After the DFT, the FD signal is mapped to the allocated bandwidth. The IFFT converts the FD signal to the SC signal in the TD. We employ a QPSK modulation scheme for the TDM based pilot signal.

III. PSA-EKF RECEIVER STRUCTURE WITH TDM AND FDM BASED PILOT SIGNALS

Since s_n denotes the sample sequence of the transmitted signal with 256QAM, the received sample sequence, r_n , is represented as $r_n = s_n e^{j\varphi_n} + w_n = f_n(\varphi_n) + w_n$. Here, φ_n and w_n are the PN and the additive white Gaussian noise component with a complex value, respectively. Fig. 2 shows the receiver structure that comprises PSA PNC in the TD and iterative EKF PNC. In the figure, the gray background blocks indicate the cancellation of the SC distortion due to puncturing and multiplexing of FDM based pilot signals.

A. PSA PNC

(1) FDM pilot multiplexing

In the case of FDM based pilot multiplexing, we estimate the PN by combining multiple Discrete Cosine Transforms (DCTs) based on the linear minimum mean square error criterion [8]. The PN at sample timing n is expressed as $e^{j\varphi} = [e^{j\varphi_0}, \dots, e^{j\varphi_{N_{FFT}-1}}]^T$. Here, superscript T denotes transposition. We use D DCTs with a length of N_{FFT} samples as $\mathbf{v}_0, \mathbf{v}_1, \dots, \mathbf{v}_{D-1}$ [8]. Each DCT is given as $v_{lu} = \cos\left(\frac{\pi l}{N_{FFT}} u\right)$ where indexes l and u take $0 \leq l < N_{FFT}$ and $0 \leq u < D$, respectively. We define weighting coefficient $\boldsymbol{\gamma} = [\gamma_0, \dots, \gamma_{D-1}]^T$ for $\mathbf{V}^{(D)} = [\mathbf{v}_0, \mathbf{v}_1, \dots, \mathbf{v}_{D-1}]$ so that the PN compensation signal is generated using linear combining of the DCT functions as $e^{-j\varphi} = \mathbf{V}^{(D)} \boldsymbol{\gamma}$. Weighting coefficient $\boldsymbol{\gamma}$ is computed from the following equation based on the least square criterion.

$$\hat{\boldsymbol{\gamma}} = \arg \min_{\boldsymbol{\gamma}} \|e^{-j\varphi} - \mathbf{V}^{(D)} \boldsymbol{\gamma}\|^2 \quad (2)$$

We estimate weighting coefficient $\hat{\boldsymbol{\gamma}}$ by employing the FDM based pilot symbols [8]. The estimate of the PN compensation signal, $e^{-j\varphi_n}$, is multiplied with the received signal.

(2) TDM pilot multiplexing

In the case of TDM pilot multiplexing, we first estimate the PN of each pilot symbol block by coherently averaging the PN of the four or five pilot symbols. Because the separation between the contiguous pilot symbol blocks is short, we estimate the PN at each data symbol position using linear interpolation of the estimated PN of both sides of the pilot symbol blocks.

B. Iterative EKF PNC

PN compensated signal $\tilde{r}_n = r_n e^{-j\varphi_n}$ is converted into FD signal \tilde{R}_k using the FFT as $\tilde{R}_k = \frac{1}{\sqrt{N_{FFT}}} \sum_{n=0}^{N_{FFT}-1} \tilde{r}_n \exp\left(-\frac{j2\pi kn}{N_{FFT}}\right)$.

(1) First iteration loop

In TDM pilot multiplexing, the FD signal is converted to a TD signal using the inverse DFT (IDFT) after subcarrier demapping. The bit sequence before LDPC decoding is demapped and the symbol estimates are generated based on the demapped bits. By multiplexing the TDM pilot symbols, the data symbols are converted to the FD signal using the DFT. After subcarrier mapping, TD signal \hat{s}_n is generated using the IFFT.

In FDM pilot multiplexing, we remove the FDM based pilot in the FD, while it is removed in the TD after IDFT together with the SC distortion as in [12] and [13]. After removing the FDM pilot, the signal including the residual PN is converted to a TD signal using the IDFT. In the first iteration loop, we first remove the SC distortion due to puncturing. Let $r_\lambda(m)$ be the IDFT output signal ($0 \leq \lambda \leq (L+Q)-1$, $0 \leq m \leq M-1$). We estimate the SC distortion due to puncturing in the $M \times L$ symbol duration where “0” signals are multiplexed at a transmitter as $\bar{r}(m) = \sum_{\lambda=1}^L r_\lambda(m)$. The estimated SC distortion is subtracted from the data symbols in the $(M \times Q)$ symbol duration as [12], [13],

$$\tilde{r}_q(m) = r_q(m) - \bar{r}(m) \quad q = 0, \dots, Q-1. \quad (3)$$

Here, $\tilde{r}_q(m) = \tilde{r}(\bar{n})$ ($0 \leq \bar{n} \leq N_D-1$). Signal $\tilde{r}_{\bar{n}}$ is demapped to recover the transmitted bit sequences before LDPC decoding based on the minimum Euclidean distance and we generate the 256QAM symbol estimates. Based on the regenerated symbol sequence, we generate the symbol sequence after adding the “0” signal in front of the data symbols as $\hat{\mathbf{u}}_t = [\mathbf{0}_{1:M \times L} \hat{\mathbf{s}}_D]$ where $\hat{\mathbf{s}}_D = [\hat{s}_D(0), \dots, \hat{s}_D(N_D-1)]$. After converting TD signal $\hat{\mathbf{s}}_D$ to an FD signal, we puncture M subcarriers and multiplex the FDM pilot for the residual PN estimation using the EKF as

$$\hat{\mathbf{S}}_f(\bar{k}) = \begin{cases} p(\bar{k}/(L+Q)) & \text{if } \bar{k} = m(L+Q), \quad m = 0, \dots, M-1 \\ \hat{u}_f(\bar{k}), & \text{otherwise} \end{cases} \quad (4)$$

Equation (4) is converted into TD signal \hat{s}_n using the IFFT.

We used an EKF to estimate the residual PN because received signal r_n is a non-linear function of the state vector

of PN φ_n at time n . By employing an accurate \hat{s}_n value, the EKF PNC can suppress the residual PN effectively. We set the initial value of the tracked PN and the model variance as $\varphi_{0|0}^{(i)} = \angle(r_0/\hat{u}_0)$ and $P_{0|0}^{(i)} = 1$, respectively, where variable i denotes the iteration index of EKF PNC. We first update the *a priori* PN and the model variance as $\varphi_{n|n-1}^{(i)} = \varphi_{n-1|n-1}^{(i)}$ and $P_{n|n-1}^{(i)} = P_{n-1|n-1}^{(i)} + Q$, respectively, where Q is the PN variance. Tracked PN error $\alpha_n^{(i)}$ is computed using the *a priori* PN in the equation below. In the first iteration of the EKF, $\tilde{u}_n^{(1)}$ is generated based on the symbol estimate after compensating for the PN using PSA PNC. In the second iteration or later, we use $\tilde{u}_n^{(i)} = \hat{u}_n^{(i-1)}$ where $\hat{u}_n^{(i)}$ is the TD signal after the IFFT based on the remapped signal at the i -th iteration of the EKF.

$$\alpha_n^{(i)} = \tilde{r}_n^{(i)} - \tilde{u}_n^{(i)} \exp(j\varphi_{n|n-1}^{(i)}) \quad (5)$$

In (5), $\tilde{r}_n^{(i)}$ is given as $\tilde{r}_n^{(1)} = r_n$ and $\tilde{r}_n^{(i)} = r_n \exp(-j\tilde{\varphi}_n^{(i-1)})$ when i is equal to two or greater. Moreover, $\tilde{\varphi}_n^{(i)}$ is defined as $\tilde{\varphi}_n^{(i)} = \tilde{\varphi}_n^{(i-1)} - \varphi_n^{(i)}$. Let $\Psi_n^{(i)}$ be the Jacobian matrix for $\tilde{r}_n^{(i)}$ as $\frac{\partial \tilde{r}_n^{(i)}}{\partial \varphi_n} = j\tilde{u}_n^{(i)} \exp(j\tilde{\varphi}_n^{(i)})$, then EKF gain $G_n^{(i)}$ is computed using the *a priori* PN and the model variance as follows.

$$G_n^{(i)} = \frac{\Psi_n^{(i)H} P_{n|n-1}^{(i)}}{|\tilde{u}_n^{(i)}|^2 P_{n|n-1}^{(i)} + \kappa} = \frac{-j\tilde{u}_n^{(i)H} \exp(-j\varphi_{n|n-1}^{(i)}) P_{n|n-1}^{(i)}}{|\tilde{u}_n^{(i)}|^2 P_{n|n-1}^{(i)} + \kappa} \quad (6)$$

In (6), κ denotes the variance of the observation noise. By using the PN error and EKF gain, the *a posteriori* PN and model variance are updated based on the *a priori* PN and variance, respectively, as shown below.

$$\begin{cases} \varphi_{n|n}^{(i)} = \varphi_{n|n-1}^{(i)} + G_n^{(i)} \alpha_n^{(i)} \\ P_{n|n}^{(i)} = (1 - j\tilde{u}_n^{(i)} \exp(j\varphi_{n|n-1}^{(i)}) G_n^{(i)}) P_{n|n-1}^{(i)} \end{cases} \quad (7)$$

The estimated PN, $e^{j\varphi_n^{(i)}}$, at sample timing n in the first iteration of the EKF is multiplied to the received signal.

(2) Second iteration loop or later

In the second iteration loop, the EKF PNC further compensates for the residual PN in the received signal. For this signal, the FDM pilot is removed in the FD after the FFT. After converting the TD signal using the IDFT, the SC distortion due to puncturing is removed. In the second iteration loop or later, the SC distortion is estimated based on the 256QAM symbol estimate using the demapped bits in the previous iteration loop. After eliminating the SC distortion due to puncturing, \hat{r}_k is demapped to recover the transmitted bit sequence. Based on the recovered bit sequence, we generate the QAM symbol sequence after adding the "0" signal in front of the data symbols as $\hat{\mathbf{u}}^t = [\mathbf{0}_{1:M \times L} \hat{\mathbf{s}}_D]$ where $\hat{\mathbf{s}}_D = [\hat{s}_D[0], \dots, \hat{s}_D[D-1]]$. The symbol sequence is converted to an FD signal using the DFT and punctured. This punctured SC signal is used to estimate the SC distortion in the next iteration loop. Simultaneously, the punctured SC signal after multiplexing the FDM pilot signal is converted to a TD signal

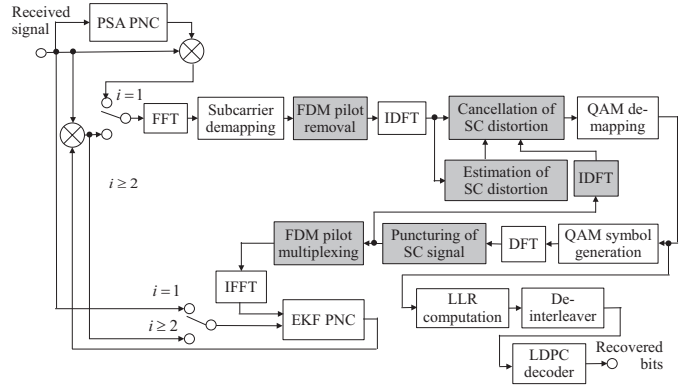


Fig. 2. PSA-EKF PNC receiver structure with TDM and FDM based pilot signals for DFT-S-OFDM.

using the IFFT. This TD signal is used as a reference signal for EKF PNC in the second iteration loop.

In the subsequent simulation, we set the number of iterations of EKF PNC to $N_{itr} = 2$. Hence, after the second iteration, we compute the log-likelihood ratio (LLR) of each bit of the 256QAM symbols based on the minimum Euclidean distance between the received symbol after the PN is compensated and the symbol replica. The computed LLR is fed into the LDPC decoder. Finally, the transmitted bit sequence is recovered at the LDPC decoder output.

IV. COMPUTER SIMULATIONS

In this paper, we employ a PN model whose power spectrum density (PSD) is given as $S_\theta(\omega) = K_\theta \frac{1+(\omega/\omega_z)^2}{1+(\omega/\omega_p)^2}$. Here, K_θ is the PN level at 0 Hz, and $f_z = \omega_z/(2\pi)$ and $f_p = \omega_p/(2\pi)$ are the zero and pole frequencies, respectively [15]. The PN is generated by passing white Gaussian noise through an infinite impulse response low-pass filter with single pole and single zero frequency. We set $f_p = 100$ Hz and $f_z = 7$ MHz [7]. We set the PSD of the PN at a frequency offset of 0 Hz, $K_\theta = -25$ dBc/Hz.

A. PAPR Performance

Fig. 3 shows the complementary cumulative distribution function (CCDF) of the PAPR of DFT-S-OFDM using the TDM and FDM pilot signals for PN estimation for 256QAM. In the case of the FDM based pilot signal, the pilot signal is multiplexed in $M = 23$ subcarrier positions every 8 subcarriers across 184 subcarriers for $L = 1$. We also plot the PAPR for DFT-S-OFDM without pilot signals. Fig. 3 shows that the PAPR at the CCDF of 10^{-4} of DFT-S-OFDM with the TDM based pilot signal decreases by approximately 0.5 dB compared to that for DFT-S-OFDM without a pilot signal. Moreover, Fig. 3 shows that the PAPR at the CCDF of 10^{-4} of DFT-S-OFDM with FDM pilot multiplexing is increased by approximately 1.8 dB and 1.2 dB compared to that for DFT-S-OFDM with TDM pilot multiplexing and that for DFT-S-OFDM without a pilot signal, respectively, for 256QAM.

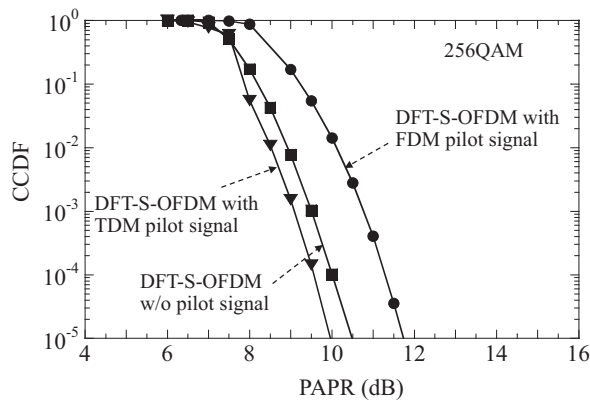


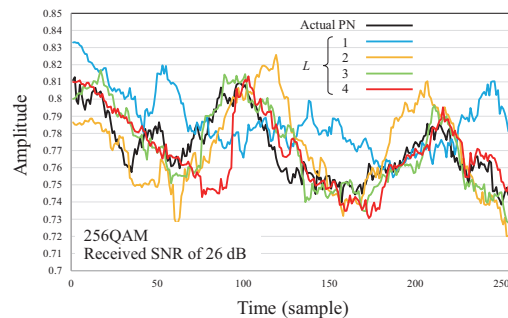
Fig. 3. PAPR of DFT-S-OFDM with TDM and FDM based pilot signals.

B. BER Performance

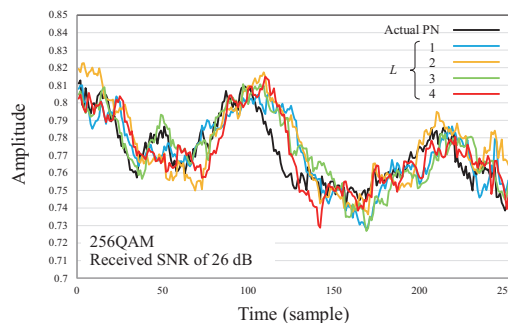
Fig. 4 shows the time variation in the estimated PN using PSA-EKF PNC along with the time-varying PN as a reference. Figs. 4(a) and 4(b) show the estimated PN using the TDM and FDM pilot multiplexing schemes, respectively. In the figures, we parameterize the L value. Fig. 4(a) shows that the estimated PN by employing PSA-EKF PNC with TDM pilot multiplexing tracks the time-varying PN more accurately according to the increase in the L value. This is because more pilot symbols are multiplexed within a DFT-S-OFDM symbol duration. Fig. 4(b) shows that the estimation error using PSA-EKF PNC with FDM pilot multiplexing compared to the actual PN is reduced according to the increase in the L value. This is due to the decrease in the SC distortion signal by puncturing because it is estimated more accurately in the first iteration loop.

Fig. 5 shows the BER of the PSA PNC only using the TDM and FDM based pilot signals for 256QAM as a function of the received signal-to-noise ratio (SNR). We parameterize the L value. The LDPC coding rate is set to $R = 8/9$. Fig. 5 shows that when using the FDM based pilot signal, no error floor is observed in a BER region as low as 10^{-8} due to the accurate tracking performance. When using the TDM based pilot signal, we find an error floor above the BER of 10^{-7} for $L = 1$. Moreover, the required received SNR at the target BER of lower than approximately 10^{-5} is increased for $L = 2$ because the tracking performance for the time-varying PN is degraded. However, when the L value is three or four, the BER is reduced directly according to the increasing received SNR because the pilot symbols are multiplexed at high density within a DFT-S-OFDM symbol. For $L = 4$, the required received SNR satisfying the BER of 10^{-8} using the FDM based pilot signal is increased by approximately 2.5 dB compared to that with the TDM based pilot signal. This is chiefly due to the residual SC distortion caused by puncturing.

Fig. 6 shows the BER of the PSA-EKF PNC using the TDM and FDM based pilot signals for DFT-S-OFDM for the 256QAM scheme with $R = 8/9$. Fig. 6 shows that the BER of PSA-EKF PNC is improved compared to only PSA PNC particularly in the case of the FDM based pilot signal. This



(a) TDM based pilot signal



(b) FDM based pilot signal

Fig. 4. Time variation of estimated PN using PSA-EKF PNC.

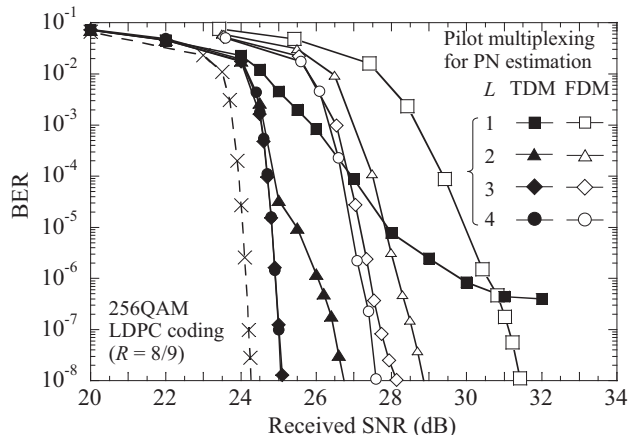


Fig. 5. BER of PSA PNC only with TDM and FDM based pilot signals for DFT-S-OFDM.

is because the SC distortion due to puncturing is reduced synergistically with the decrease in the residual PN by the iterative EKF PNC. We observe degradation in the BER for the TDM pilot multiplexing for $L = 1$ and 2 in the BER region of lower than approximately 10^{-5} . Nevertheless, the BER is reduced steeply for $L = 3$ and 4. With $L = 4$, the required received SNR of the PSA-EKF PNC using the TDM based pilot signal is decreased by approximately 1.2 dB compared to that using the FDM based pilot signal for 256QAM.

Fig. 7 shows the BER of the PSA-EKF PNC using the TDM and FDM based pilot signals with the LDPC coding rate of $R = 1/2, 3/4, \text{ and } 8/9$. We set $L = 4$. Fig. 7 shows that the BER

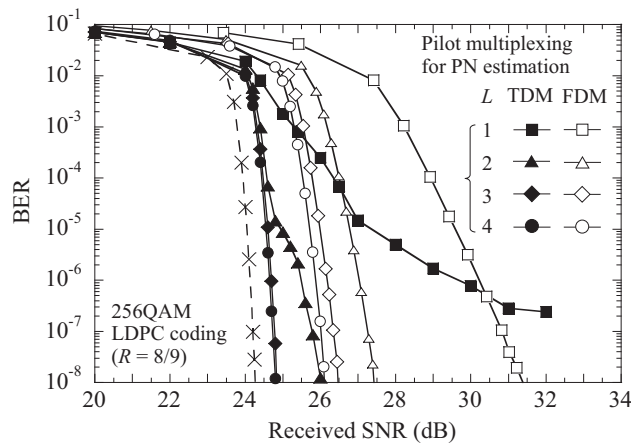


Fig. 6. BER of PSA-EKF PNC using TDM and FDM based pilot signals with $R = 8/9$ for DFT-S-OFDM.

of PSA-EKF PNC with the TDM based pilot signal is better than that with the FDM based pilot signal regardless of the R value. We see that the required received SNR satisfying the BER of 10^{-8} with the TDM based pilot signal is decreased by approximately 1.1 dB, 1.2 dB, and 1.3 dB compared to that with the FDM based pilot signal for $R = 1/2$, $3/4$, and $8/9$, respectively. For $L = 3$ and 4 , the pilot insertion ratio within a DFT-S-OFDM symbol is approximately 30% and 36%, respectively. In the case of $L = 4$, the number of data symbols between the contiguous pilot blocks is only 8. Hence, it is rational to think that the TDM pilot multiplexing can track the PN accurately. This result suggests that a more accurate estimation method of the SC distortion that can decrease the L value is necessary for FDM based pilot signal multiplexing. We note that the TDM based pilot signal for PN estimation is applicable to point-to-point transmission including mobile backhaul links and the broadcast channel in the downlink access link. However, in uplink multi-access channels, PN estimation incurring high complexity is necessary because PN

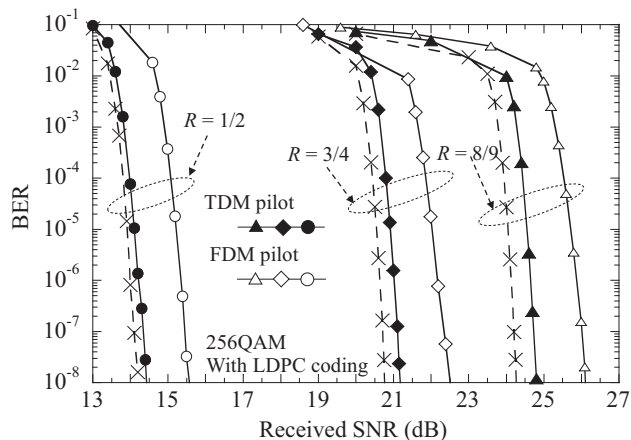


Fig. 7. BER of PSA-EKF PNC using TDM and FDM based pilot signals with LDPC coding rate of $R = 1/2$, $3/4$, and $8/9$ for DFT-S-OFDM.

estimation is only possible after separating the other UE uplink channels.

V. CONCLUSION

This paper presented comparisons of TDM and FDM based pilot signal multiplexing schemes for estimating the time-varying PN with high-order QAM for DFT-S-OFDM. Computer simulation results showed that the PAPR at the CCDF of 10^{-4} of DFT-S-OFDM with FDM pilot multiplexing is increased by approximately 1.8 dB and 1.2 dB compared to that for DFT-S-OFDM with TDM pilot multiplexing and that for DFT-S-OFDM without a pilot signal, respectively, for 256QAM. We showed that the required received SNR satisfying the BER of 10^{-8} with a TDM based pilot signal is decreased by approximately 1.1 dB, 1.2 dB, and 1.3 dB compared to that with a FDM based pilot signal employing LDPC coding with $R = 1/2$, $3/4$, and $8/9$, respectively, for 256QAM. Therefore, we show that the TDM based pilot signal for the PN estimation achieves superior performance to the FDM based one, while the FDM based pilot signal has the potential for improvement if elaborate cancellation of the SC distortion due to puncturing is employed.

ACKNOWLEDGMENT

This research and development work was supported by MIC/SCOPE JP225003003. We thank Dr. Norifumi Kamiya of the Advanced Network Research Laboratories, NEC Corporation for his invaluable technical contributions to our research.

REFERENCES

- [1] 3GPP TS 38.211, "NR; Physical channels and modulation (Release 15)," V1.2.0, Nov. 2017.
- [2] C. Johnson, 5G New Radio in Bullets, 2019.
- [3] 3GPP TR 38.874, "Study on integrated access and backhaul," V16.0.0, Dec. 2018.
- [4] G. Berardinelli, K. I. Pedersen, T. B. Sorensen, and P. Mogensen, "Generalized DFT-spread-OFDM as 5G waveform," IEEE Commun. Mag., vol. 54, no. 11, pp. 99 - 105, Nov. 2016.
- [5] H. Nikopour, *et al.*, "Single carrier waveform solution for millimeter wave air interface," Proc. 2016 IEEE Globecom Workshops, Dec. 2016.
- [6] C. -T. Lam, D. D. Falconer, and F. D. - Lemoine, "Iterative frequency domain channel estimation for DFT-precoded OFDM systems using in-band pilots," IEEE Journal on Selected Areas in Communications, vol. 26, no. 2, pp. 348 - 358, Feb. 2008.
- [7] N. Kamiya and E. Sasaki, "Pilot-symbol assisted and code-aided phase error estimation for high-order QAM transmission," IEEE Trans. on Commun., vol. 61, no. 10, pp. 4369-4380, Oct. 2013.
- [8] R. A. Casas, S. L. Biracree, and A. E. Youtz, "Time domain phase noise correction for OFDM signals," IEEE Trans. on Broadcasting, vol. 48, no. 3, pp. 230 - 236, Sept. 2002.
- [9] R. Kuribayashi, M. Sawahashi, and N. Kamiya, "Phase noise compensation using FDM based pilot symbol assisted EKF for OFDM based radio backhaul links," Proc. IEEE PIMRC2022, Sept. 2022.
- [10] R. Kuribayashi and M. Sawahashi, "Phase noise estimation and compensation using FDM pilot for high-order QAM transmission for DFT-spread OFDM backhaul links," Proc. IEEE VTC2023-Fall, Oct. 2023.
- [11] ETSI EN 302 307, "Second generation framing structure, channel coding, and modulation systems for DVB-S2," April 2009.
- [12] A. Sahin, E. Bala, R. Yang, and R. L. Olesen, "DFT-spread OFDM with frequency domain reference symbols," Proc. IEEE Globecom 2017.
- [13] T. PS Chandrashekhar, S. Amuru, J. Nair, and A. Guchhait, "Multiplexing reference signals and data in a DFT-s-OFDM symbol," Proc. IEEE SPCOM 2018.
- [14] D. C. Chu, "Polyphase codes with good periodic correlation properties," IEEE Trans. Inform. Theory, vol. IT-18, pp. 531 - 532, July 1972.
- [15] C.-S. Choi, *et al.*, "RF impairment models for 60GHz-band SYS/PHY simulation," IEEE document 802.15-06-0477-01-003c, Nov. 2006.